# Theory and simulation of high-gain ion-ripple lasers

K. R. Chen* and J. M. Dawson
*Department of Physics, University of California at Los Angeles, Los Angeles, California 90024*
(Received 21 October 1991)

Both the Raman, coherent Compton, and Compton regimes of high-gain ion-ripple Lasers (IRL's) are studied. The IRL works by coupling a negative-energy beam wave (or ponderomotive potential) to an electromagnetic wave by means of the ion ripple (backward Raman scattering or backward coherent Compton scattering) or by amplification of an em wave by negative Landau damping (backward Compton scattering). By employing fluid theory, the dispersion relation for wave coupling is derived and used to calculate the radiation frequency and linear growth rate. The nonlinear saturation mechanism is explored. A multidimensional (one dimension in space, three dimensions in momenta and fields) particle-in-cell simulation code was developed to verify the ideas, scaling laws, and nonlinear mechanisms. The effect of momentum spread is also studied; there is a slow decrease in the growth rate and efficiency as well as broadening of the radiation spectrum. This scheme may provide tunable sources of coherent high-power radiation. By proper choice of device parameters, sources of microwaves, optical, and perhaps even x rays can be made. An ion ripple in a plasma can provide a very short undulator wavelength (e.g., $\sim 10^{-2}$ cm) and strong dc electric fields (e.g., $\sim 10^{10}$ V/m; equivalent to a magnetic field of 30 T). The plasma also produces an ion channel that provides guiding of electron and laser beams. The IRL's may generate high-power (e.g., $>1$ MW), coherent, short-wavelength photons with relatively low beam energy (e.g., $\sim 10$ MeV) and possibly low beam quality requirement. The availability of tunable sources for wide wavelength regimes, coherence and high power, as well as lower cost and simplicity of equipment are emphasized.

PACS number(s): 41.60.Cr, 52.35.Fp, 52.40.Mj, 52.65.+z

## I. INTRODUCTION

A scheme [1] to generate tunable coherent radiation in a high-gain regime is studied here. The basic concept is to use a relativistic electron beam propagating obliquely across an ion ripple, as shown in Fig. 1. Electromagnetic radiation is generated with a peak growth rate at a resonance frequency, $\omega \sim 2\gamma_0^2 k_{\rm ir} c \cos\theta$, where $\gamma_0$ is the beam's Lorentz factor, $k_{\rm ir}$ is the wave number of the ion ripple, and $\theta$ is the angle between the beam and the ripple.

The first step is to create a plasma density ripple. As one possibility, a sound wave can be used to modulate the density of a neutral gas which is then ionized by a laser pulse [2]. The wavelength of the gas ripple is limited by the molecular mean free path (it should be $>10\lambda_{\rm MFP}$). The mean free path can be estimated from

$$\lambda_{\rm MFP} \simeq (\pi A^2 n_g)^{-1} , \tag{1}$$

where $A$ is the radius of a gas molecule and $n_g$ is the gas number density. Thus a shorter ripple length can be obtained by using higher gas densities and larger atoms or molecules. The amplitude of such density ripple can be large ($\sim 50\%$) for realistic situations. Another way to create the ion ripple is to excite an ion acoustic wave [3] in the plasma. The wave number and frequency of the plasma ripple are those of an ion acoustic wave:

$$\omega_{\rm ir} = \frac{\omega_{pi}}{(1+1/k_{\rm ir}^2 \lambda_{De}^2)^{1/2}} , \tag{2}$$

where $\omega_{\rm ir}$ is the frequency, $\omega_{pi}$ is the ion plasma frequency, $k_{\rm ir}$ is the wave number, and $\lambda_{De}$ is the electron Debye length. For $k_{\rm ir}\lambda_{De} \ll 1$, we get the wave number to be

$$k_{\rm ir} = \omega_{\rm ir}/c_s , \tag{3}$$

where $c_s = (\kappa T_e/m_i)^{1/2}$ is the ion acoustic speed, $\kappa T_e$ is the plasma electron temperature, and $m_i$ is the ion mass. We have assumed the ion temperature is low. The ion ripple is shielded by plasma electrons.

In order to produce radiation from the ion ripple, a relativistic electron beam is injected into the plasma at an

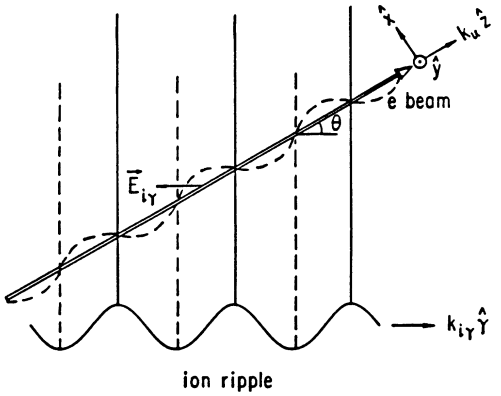


FIG. 1. A relativistic electron beam propagates through an ion ripple with an angle $\theta$. The dashed curve is the actual beam electrons' trajectory, while the straight arrow is the original beam path. The radiation direction is the beam direction.

 

angle $\theta$ with respect to the ripple. As long as the beam density $n_b$ is equal to, or higher than, the plasma density $n_0$, the plasma electrons are expelled from the path of electron beam [4,5] by its space charge. The ion ripple will then be seen as a stationary undulating force by the beam electrons. The electron oscillation frequency caused by the undulated force is $k_{ir}v_0\cos\theta$, where $v_0$ is the beam velocity.

We take the density of the ion ripple to be

$$n_i = n_0[1+\epsilon_{ir}\sin(k_{ir}r)] , \tag{4}$$

where $\epsilon_{ir}$ is the fractional perturbation ripple density. The ion ripple is assumed to be stationary because the interaction time scale is much shorter than that for ion motion. The electric field induced by this ion ripple is that produced by unshielded ions because the plasma electrons are expelled and the beam is so stiff it does not shield the ions; therefore it is

$$\mathbf{E}_{ir} = -\frac{4\pi n_0 e}{k_{ir}}\epsilon_{ir}\cos(k_{ir}r)\hat{\mathbf{r}} , \tag{5}$$

where $\hat{\mathbf{r}}$ is the ripple direction (we assume the beam density is equal to or greater than the plasma density).

Since the beam velocity $v_0$ is much greater than the acoustic velocity $c_s$, the ion ripple can be treated as stationary. If the transverse ($\hat{\mathbf{x}}$ and $\hat{\mathbf{y}}$) variation of the ion-ripple field on the beam electrons is negligible, as shown in Fig. 1, the problem can be simplified to one dimension. The electric field acting upon the beam can be written as

$$\mathbf{E}_{ir} = \frac{4\pi n_0 e}{k_u}\epsilon_i\cos(k_u z)(\hat{\mathbf{x}}\sin\theta - \hat{\mathbf{z}}\cos\theta) , \tag{6}$$

where $\epsilon_i = \epsilon_{ir}\cos\theta$ is the fractional ripple of ion density, and $k_u = k_{ir}\cos\theta$ is the effective wave number of the ion ripple along the beam direction. The longitudinal ($\hat{\mathbf{z}}$) part of $\mathbf{E}_{ir}$ may excite electrostatic instabilities [6,7] on the beam. However, since the time scale of the electromagnetic (em) radiation growth is much shorter than that of the electrostatic (es) waves, this becomes unimportant if [6]

$$k_u c \gg \frac{\omega_{pe}}{\gamma_0^{3/2}} , \tag{7}$$

where $\omega_{pe}^2 = 4\pi n_0 e^2/m_e$ is the plasma frequency. This will be checked in the computer simulation. Subjected to the transverse ($\hat{\mathbf{x}}$) field of $\mathbf{E}_{ir}$, the beam electrons execute transverse oscillations. These transverse oscillations are the source of the energy needed to produce electromagnetic radiation[8].

The low-gain regime for the ion-ripple laser (IRL) can be described by the unified theory of our previous paper [8]. There the IRL is treated as an initial-value problem and the amplitude of the radiation wave field is approximated to be a constant. In this paper, we are going to study the ion-ripple laser in the high-gain regime, where collective effects are important. The dispersion relation will be derived in the following section using Fourier analysis. Section III studies the ion-ripple laser in the Raman regime (collective space-charge effects are important); while the coherent Compton regime (collective space-charge effects are negligible, but the electron motion is coherent) will be divided into two domains according to the undulator length and will be discussed in Sec. IV. In the long-undulator-wavelength domain for the high-gain coherent Compton regime, we will see that the transverse electron oscillations are much stronger than those in the short-undulator-wavelength domain due to the magnetic field associated with the equilibrium oscillatory motion of the beam. The simulation model we developed in an our paper [10] is used to check the validity of the theory and to study the nonlinear saturation mechanisms; the results are shown in Sec. V. Possible applications are discussed and comparisons made with the free-electron laser [11]–[29] in Sec. VI. Section VII gives a summary and some discussion.

## II. THEORY AND DISPERSION RELATION

In the low-gain regime, the energy gain of wave fields is small comparing with the initial energy of the waves. The amplitude of wave fields can be assumed to be a constant during the interaction. This is usually true for early times in the interaction. The interaction can be studied as an initial-value problem. However, in the high-gain regime, the wave fields gain a lot of energy; the amplitude of the wave can grow exponentially. The motion of the beam electrons is also strongly modulated by the growth of the wave fields. Thus it is necessary to study the interaction self-consistently; that is, a dispersion relation needs to be derived. Fourier analysis is the natural way to attack this problem.

The equations needed to derive the dispersion relation are Maxwell equations, the continuity equation, and the equation for electron motion. They are given by

$$\nabla_z \cdot E_z = 4\pi(n_i - n_b)e , \tag{8}$$

$$\nabla_z \times E_x = -\frac{1}{c}\frac{\partial B_y}{\partial t} , \tag{9}$$

$$\nabla_z \times B_y = \frac{4\pi}{c}j_x + \frac{1}{c}\frac{\partial E_x}{\partial t} , \tag{10}$$

$$0 = \frac{\partial n_b}{\partial t} + \frac{P_z}{\gamma m_e}\frac{\partial n_b}{\partial z} + \frac{n_b}{m_e}\frac{\partial}{\partial z}\left[\frac{P_z}{\gamma}\right] , \tag{11}$$

$$\frac{d}{dt}\mathbf{P} = -e\left[\mathbf{E} + \frac{\mathbf{P}\times\mathbf{B}}{\gamma m_e c}\right] - \frac{3\kappa T}{n_b}\frac{\partial n_b}{\partial z}\hat{\mathbf{z}} , \tag{12}$$

where $E_x$, $E_z$, and $\mathbf{E}$ are the electric fields, $B_y$ and $\mathbf{B}$ are the magnetic fields, $j_x = -n_b e v_x$ is the transverse current of the electron beam, $m_e$ is the rest mass of the electron, $P_x = \gamma m_e v_x$, $P_z = \gamma m_e v_z$, and $\mathbf{P} = \hat{\mathbf{x}}P_x + \hat{\mathbf{z}}P_z$ are the momentum components of the beam electron, and $\kappa T$ is the beam electron temperature and is assumed small (if it is not small, a pressure tensor or a covariant formalism [30] shall be used). We have taken the beam density to be, on average, equal to the plasma (ion) density to simplify the analysis; we could of course carry through the analysis for other situations. The wave fields induced by

the charge density and current are given by Maxwell equations [Eqs. (8)–(10)]. The electron's response to the wave fields is described by the equation of motion [Eq. (12)]. The continuity equation [Eq. (11)] assures the conservation of beam charge and provides a relation between the perturbations of the charge density and longitudinal velocity. The momentum transfer between the longitudinal and transverse motion is via $\mathbf{j}\times\mathbf{B}$, which provides a ponderomotive force.

To simplify the algebraic calculation, we use the following dimensionless scales:

$$\begin{aligned}
&t\leftarrow\omega_{pe}t\ ,\\
&x,z\leftarrow x\omega_{pe}/c,z\omega_{pe}/c\ ,\\
&n_i,n_e\leftarrow n_i/n_0,n_e/n_0\ ,\\
&P_x,P_z\leftarrow P_x/(m_ec),P_z/(m_ec)\ ,\\
&T\leftarrow\kappa T/m_ec^2\ ,\\
&E_x,E_z,B_y\\
&\qquad\leftarrow eE_x/(m_e\omega_{pe}c),eE_z/(m_e\omega_{pe}c),eB_y/(m_e\omega_{pe}c)\ .
\end{aligned}\tag{13}$$

Then, Eqs. (8)–(12) become

$$\frac{\partial}{\partial z}E_z=n_i-n_b\ ,\tag{14}$$

$$\frac{\partial}{\partial z}E_x=-\frac{\partial}{\partial t}B_y\ ,\tag{15}$$

$$\frac{\partial}{\partial z}B_y=-j_x-\frac{\partial}{\partial t}E_x\ ,\tag{16}$$

$$0=\frac{\partial}{\partial t}n_b+\beta_z\frac{\partial}{\partial z}n_b+n_b\frac{\partial}{\partial z}\beta_z\ ,\tag{17}$$

$$\frac{d}{dt}\mathbf{P}=-(\mathbf{E}+\boldsymbol{\beta}\times\mathbf{B})-3T\frac{\partial n_b}{\partial z}\hat{\mathbf{z}}\ ,\tag{18}$$

where $\beta_z=v_z/c$ and $\boldsymbol{\beta}=\mathbf{v}/c$.

If we assume $\epsilon_i\ll 1$, then the equilibrium state (including the ion-ripple fields ) is given by

$$n_{b0}=n_0[1+\epsilon_e\sin(k_uz)]\ ,\tag{19}$$

$$P_{z0}=P_0[1-\gamma_0^2\epsilon_e\sin(k_uz)]\hat{z}\ ,\tag{20}$$

$$P_x=\gamma_0\beta_u\sin(k_uz)\hat{x}\ ,\tag{21}$$

$$B_{y0}=-\frac{\beta_u}{k_u}\cos(k_uz)\hat{y}\ ,\tag{22}$$

$$\gamma_{00}=\gamma_0[1-\gamma_0^2\beta_0^2\epsilon_e\sin(k_uz)]\ ,\tag{23}$$

$$\beta_u=-\frac{1/\gamma_0}{\beta_0^2/\gamma_0+k_u^2\beta_0^2}\epsilon_i\sin\theta\ ,\tag{24}$$

$$\epsilon_e=\frac{1/\gamma_0^3}{(1+3k_u^2\beta_t^2)/\gamma_0^3-k_u^2\beta_0^2}\epsilon_i\cos\theta\ ,\tag{25}$$

where $P_0=\gamma_0\beta_0$ is the initial beam momentum, $\beta_0=v_0/c$, $\beta_t=v_t/c$, and $v_t$ is the electron thermal velocity.

For small-amplitude electrostatic and electromagnetic waves ($E_x,E_z\ll|\mathbf{E}_{ir}|$), perturbation theory can be used. The first- order equations (for the perturbed fields) of Eqs. (14)–(18) can be obtained by a perturbation expansion using the equilibrium state:

$$\frac{\partial}{\partial z}E_z=-n\ ,\tag{26}$$

$$\left[\frac{\partial^2}{\partial z^2}-\frac{\partial^2}{\partial t^2}\right]E_x=-\beta_u\frac{\partial n}{\partial t}\sin k_uz-\frac{1}{\gamma_0}\frac{\partial P_x}{\partial t}+\frac{\beta_0\beta_u}{\gamma_0}\frac{\partial P_z}{\partial t}\sin k_uz\ ,\tag{27}$$

$$\frac{\partial}{\partial t}B_y=-\frac{\partial}{\partial z}E_x\ ,\tag{28}$$

$$\left[\frac{\partial}{\partial t}+\beta_0\frac{\partial}{\partial z}\right]n=-\frac{1}{\gamma_0^3}\frac{\partial}{\partial z}P_z\ ,\tag{29}$$

$$\left[\frac{\partial}{\partial t}+\beta_0\frac{\partial}{\partial z}\right]P_x=-E_x+\beta_0B_y-\frac{\beta_u}{\gamma_0^3k_u}P_z\cos k_uz\ ,\tag{30}$$

$$\left[\frac{\partial}{\partial t}+\beta_0\frac{\partial}{\partial z}\right]P_z=-E_z-\beta_uB_y\sin k_uz+\frac{\beta_u}{\gamma_0k_u}P_x\cos k_uz-3T\frac{\partial n}{\partial z}\ ,\tag{31}$$

where the dependent variables ($E_x$, $B_y$, $E_z$, $n$, $P_x$, and $P_z$) are first-order terms. Let us further restrict our considerations to $k_uv_0\gg\omega_{pe}/\gamma_0^{3/2}$, then $\epsilon_e$ is very small and we can neglect products of $\epsilon_e$ and first-order terms. We will also neglect terms which are of order $\epsilon_i^2$ times first-order terms in solving these equations. At the moment we have six equations, six dependent variables, and two independent variables $(t,z)$. Since the functions $\sin k_uz$ and $\cos k_uz$ in the equations are periodic, the dependent variables must also have this periodicity. We therefore look for solutions of the form

$$\alpha=e^{i(kz-\omega t)}\sum_{l=-\infty}^{\infty}\alpha_{k+lk_u}e^{ilk_uz}\ ,\tag{32}$$

where $\alpha$ stands for any one of the six dependent variables. We know that

$$(\alpha\cos k_uz)_k=\tfrac{1}{2}(\alpha_{k-k_u}+\alpha_{k+k_u})\ ,\tag{33}$$

$$(\alpha\sin k_uz)_k=-\frac{i}{2}(\alpha_{k-k_u}-\alpha_{k+k_u})\ .\tag{34}$$

Thus, for a particular mode $k$, Eqs. (26)–(31) become

$$E_{z,k}=\frac{i}{k}n_k\ ,\tag{35}$$

$$B_{y,k}=\frac{k}{w}E_{x,k}\ ,\tag{36}$$

$$n_k=\frac{k}{\gamma_0^3(\omega-k\beta_0)}P_{z,k}\ ,\tag{37}$$

$$(\omega^2-k^2)E_{x,k}=\frac{\omega\beta_u}{2}(n_{k-k_u}-n_{k+k_u})+\frac{i\omega}{\gamma_0}P_{x,k}-\frac{\omega\beta_u\beta_0}{2\gamma_0}(P_{z,k-k_u}-P_{z,k+k_u}) , \tag{38}$$

$$(\omega-k\beta_0)P_{x,k}=-i\left[\frac{\omega-k\beta_0}{\omega}\right]E_{x,k}-\frac{i\beta_u}{2k_u}\left[\frac{\omega-(k-k_u)\beta_0}{k-k_u}n_{k-k_u}-\frac{\omega-(k+k_u)\beta_0}{k+k_u}n_{k+k_u}\right] , \tag{39}$$

$$(\omega-k\beta_0)P_{z,k}=\frac{1+3k^2\beta_t^2}{k}n_k-\frac{\beta_u}{2\omega}[(k-k_u)E_{x,k-k_u}-(k+k_u)E_{x,k+k_u}]+\frac{i\beta_u}{2\gamma_0k_u}(P_{x,k-k_u}+P_{x,k+k_u}) , \tag{40}$$

where we have already used Eqs. (36) and (37) in obtaining Eq. (39), and Eqs. (35) and (36) in getting Eq. (40). Here the six equations for six dependent variables have been reduced to four equations [Eqs. (37)–(40)] for four dependent variables. We need to further simplify them.

Substituting Eqs. (37) and (39) into Eqs. (38) and (40), and changing the subscript of the density perturbation, we obtain

$$\left[\omega^2-k^2-\frac{1}{\gamma_0}\right]E_{x,k}=\frac{\omega\beta_u}{2}\left\{\left[1-\frac{\omega-(k-k_u)\beta_0}{k-k_u}\left[\gamma_0^2\beta_0-\frac{1}{\gamma_0k_u(\omega-k\beta_0)}\right]\right]n_{k-k_u}-\left[1-\frac{\omega-(k-k_u)\beta_0}{k-k_u}\left[\gamma_0^2\beta_0+\frac{1}{\gamma_0k_u(\omega-k\beta_0)}\right]\right]n_{k+k_u}\right\} , \tag{41}$$

$$\left[[\omega-(k\pm k_u)\beta_0]^2-\frac{1+3(k\pm k_u)^2\beta_t^2}{\gamma_0^3}\right]\times\begin{Bmatrix}n_{k+k_u}\\n_{k-k_u}\end{Bmatrix}=-\frac{(k\pm k_u)\beta_u}{2\gamma_0^3\omega}\left[\left[k\begin{Bmatrix}+0\\-2k_u\end{Bmatrix}-\frac{1}{\gamma_0k_u}\right]\times\begin{Bmatrix}E_{x,k}\\E_{k-2k_u}\end{Bmatrix}-\left[k\begin{Bmatrix}+2k_u\\-0\end{Bmatrix}+\frac{1}{\gamma_0k_u}\right]\times\begin{Bmatrix}E_{k+2k_u}\\E_{x,k}\end{Bmatrix}\right] . \tag{42}$$

The left-hand-side term of Eq. (41) is the dispersion relation of the electromagnetic mode with a wave number $k$ in a uniform electron beam. The electric-field perturbation has a current density perturbation (which is proportional to the electron density perturbation) as its source terms. Their electron density and em wave numbers differ by $k_u$, they are coupled through the ion ripple. The dispersion relation for an electrostatic mode with a wave number $k+k_u$ or $k-k_u$ in the uniform electron beam is the coefficient of $n_{k\pm k_u}$ on the left-hand side of Eq. (42); the electric-field perturbation couples to it via the current variations due to the ion ripple.

Substituting Eq. (42) into Eq. (41), we obtain the dimensionless dispersion relation

$$\left[\omega^2-k^2-\frac{1}{\gamma_0}\right]\left[[\omega-(k\pm k_u)\beta_0]^2-\frac{1+3(k\pm k_u)^2\beta_t^2}{\gamma_0^3}\right]=\frac{\left[k\mp\frac{1}{\gamma_0k_u}\right](k\pm k_u)\beta_u}{4\gamma_0^3}\left[1-\frac{\omega-(k\pm k_u)\beta_0^2}{k\pm k_u}\left[\gamma_0^2\beta_0+\frac{1}{\gamma_0k_u^2\beta_0}\right]\right] , \tag{43}$$

where the upper (lower) sign is for the upper (lower) half $\omega$ plane. Choosing the upper sign and making use of the dimension scales, we rewrite the dispersion relation as

$$\varepsilon_{em}\varepsilon_{es}=C_f , \tag{44}$$

where

$$\varepsilon_{em}=\omega^2-k^2c^2-\frac{\omega_{pe}^2}{\gamma_0} , \tag{45}$$

$$\varepsilon_{es}=(\omega-k_pv_0)^2-\frac{\omega_{pe}^2+3k_p^2v_t^2}{\gamma_0^3} , \tag{46}$$

$$C_f=\frac{\left[k-\frac{\omega_{pe}^2}{\gamma_0k_uc^2}\right]k_p\beta_u^2\omega_{pe}^2}{4\gamma_0^3}\times\left[1-\frac{\omega-k_pv_0}{k_pc}\left[\gamma_0^2\beta_0+\frac{\omega_{pe}^2}{\gamma_0k_u^2v_0c}\right]\right] , \tag{47}$$

$$\beta_u = -\frac{\omega_{pe}^2/\gamma_0}{(\omega_{pe}^2/\gamma_0)\beta_0^2 + k_u^2 v_0^2}\epsilon_i \sin\theta \ . \tag{48}$$

$\varepsilon_{em}=0$ is the dispersion relation for electromagnetic modes in a uniform plasma; $\varepsilon_{es}=0$ is the dispersion relation for electrostatic modes for wave numbers $k_p = k + k_u$ (conservation of momentum) in a uniform plasma. The wave frequency can be determined by the intersection of the electromagnetic and electrostatic dispersion curves; that is, $\omega_{em}=\omega_{es}$ (conservation of energy), where $\omega_{em}=(k^2c^2+\omega_{pe}^2/\gamma_0)^{1/2}$ is the frequency of the em mode, and $\omega_{es}(\pm)=k_p v_0 + S$, $S=\pm|S|$, and $|S|=(\omega_{pe}^2 + 3k_p^2 v_t^2)^{1/2}/\gamma_0^{3/2}$ is the frequency of fast (+) and slow (−) electrostatic beam modes. $C_f$ in Eq. (44) is understood as the coupling factor of em modes and es modes through the ion-ripple pump mode. It gives a small variation to the radiation frequency and it gives a finite bandwidth of unstable modes.

## III. HIGH-GAIN RAMAN REGIME OF THE ION-RIPPLE LASER

In this section, we analyze the growth rate and efficiency of the ion-ripple laser in the high-gain Raman regime. In the high-gain regime, the wave fields grow significantly. The wave-field growth and electron's dynamics need to be studied self-consistently. In the Raman regime, the space-charge effect is important; this separates the slow and the fast space-charge modes. We know that the radiant wave frequency can be estimated from the intersection of electromagnetic and electrostatic dispersion curves. For $\gamma \gg 1$, the wave number of the em mode is $k \sim 2\gamma_0^2(k_{ir}v_0\cos\theta + S)/c$. This reveals the scaling of the radiation frequency, including Doppler shifts and space-charge effects. The mode is called the backward Raman instability since, in the beam frame, the undulator field looks like an incoming wave and the radiation is in the opposite direction.

To obtain the growth rate and more accurate radiation wave frequency, we need to solve the dispersion relation, Eq. (44). From resonance of the slow electrostatic mode with the electromagnetic mode, we have

$$\omega - (k_p v_0 - |S|) = \delta \tag{49}$$

$$= \Delta\omega + \Delta \sim 0 \ , \tag{50}$$

$$\Delta\omega = \omega - \omega_{em} \ , \tag{51}$$

$$\Delta = \omega_{em} - k_p v_0 + |S| \ . \tag{52}$$

The dispersion relation can be rewritten as

$$\Delta\omega(\delta - 2|S|)(\Delta\omega + \Delta) = \frac{C_f}{2\omega_{em}} \ . \tag{53}$$

Since space charge is important, we assume $|S| \gg |\delta|$; that is, the slow mode is decoupled from the fast mode. Then, Eq. (53) becomes

$$\Delta\omega^2 + \Delta\,\Delta\omega + \frac{C_f}{4|S|\omega_{em}} = 0 \ . \tag{54}$$

There are complex conjugate solutions of $\Delta\omega$ if

$$\frac{C_f}{|S|\omega_{em}} > \Delta^2 \ . \tag{55}$$

Therefore the radiation frequency is

$$\omega = \omega_r + i\omega_i \ , \tag{56}$$

$$\omega_r = \omega_{em} - \frac{\Delta}{2} \ , \tag{57}$$

$$\omega_i = \tfrac{1}{2}\left[-\Delta^2 - \frac{C_f}{S\omega_{em}}\right]^{1/2} \ , \tag{58}$$

where $\Delta = \omega_{em} - \omega_{es}$. We define $\delta_r = \omega_r - \omega_{es} = \Delta/2$ as the mismatch factor including space-charge effects [8].

Equation (57) reveals that the radiation frequency is halfway between the frequencies of the uncoupled electromagnetic wave mode and the slow electrostatic beam mode as shown in Fig. 2. This is a characteristic for two-wave coupling.

Resonance occurs at $\delta \sim 0$ so that the condition for instability can be expressed by $C_f S < 0$. This can be explained as follows. We rewrite the dispersion relation, Eq. (44), to read

$$(\omega^2 - \omega_{em}^2)[\omega - \omega_{es}(+)][\omega - \omega_{es}(-)] = C_f \ . \tag{59}$$

When the slow electrostatic beam mode and the backward scattered em mode are at resonance [i.e., $\omega - \omega_{es}(-) \sim \delta$ and $\omega - \omega_{es}(+) \sim 2S < 0$], as $\delta < 0$ $(>0)$ the requirement for resonance is $\omega^2 - \omega_{em}^2 > 0$ $(<0)$, which can be understood from the $\omega$-$k$ diagram (Fig. 2). Thus the coupling factor needs to be positive; that is, $C_f S < 0$. In other words, we can find a solution between the electromagnetic wave mode and the slow space-charge mode [$\omega_{em} > \omega > \omega_{es}(-)$ or $\omega_{es}(-) > \omega > \omega_{em}$], but there is no solution between the fast space-charge mode and the electromagnetic wave mode [$\omega_{em} > \omega > \omega_{es}(+)$ or $\omega_{es}(+)$

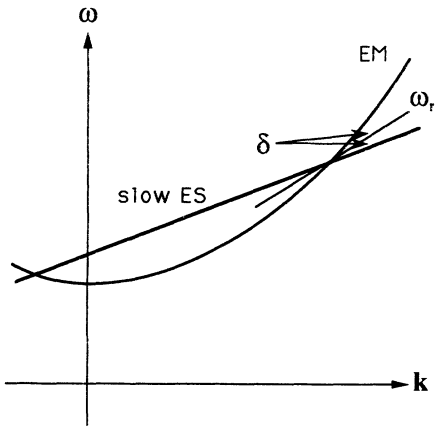


FIG. 2. The radiation frequency is midway between that of the electromagnetic mode (EM) and the slow space-charge mode (ES).

$> \omega > \omega_{em}$] to satisfy the dispersion relation.

The bandwidth of the spectrum can be estimated from the coupling factor $C_f > |S|\omega_{em}\Delta^2$; that is, the waves coupling should overcome the mismatch. As shown in Fig. 3, when the coupling factor increases (e.g., by increasing the amplitude of the ion ripple $\epsilon_i$ and hence the transverse velocity), the unstable bandwidth becomes broader and the maximum growth rate increases.

The maximum growth rate is at $\Delta=0$; that is,

$$\omega_{i,\max}=\frac{1}{2}\left[\frac{C_f}{|S|\omega_{em}}\right]^{1/2} . \tag{60}$$

For an energetic electron beam, $\gamma \gg 1$, the maximum growth rate is

$$\frac{\omega_{i,\max}}{\omega_{pe}}=\frac{1}{2}\left[\frac{\beta_u^2}{2}\frac{\sqrt{\gamma_0}k_u c}{\omega_{pe}}\right]^{1/2} , \tag{61}$$

where the growth rate depends on the transverse oscillation velocity. The transverse oscillation velocity depends on the plasma (and beam) density. If $k_u c \gg \omega_{pe}/\gamma_0^{1/2}$, the maximum growth rate becomes

$$\frac{\omega_{i,\max}}{\omega_{pe}} \simeq \left[\frac{\omega_{pe}}{\sqrt{\gamma_0}k_u c}\right]^{3/2}\frac{\epsilon_i \sin\theta}{2\sqrt{2}} , \tag{62}$$

the growth rate is inversely proportional to $\gamma_0^{3/4}$.

The nonlinear saturation mechanism of the ion-ripple laser is expected to be due to trapping of beam electrons in the electrostatic potential wells of the beam plasma wave. The mean velocity of the beam electrons after trapping is the phase velocity of the slow space-charge wave. The average energy of the beam after trapping will be $\gamma_{ph}$, where

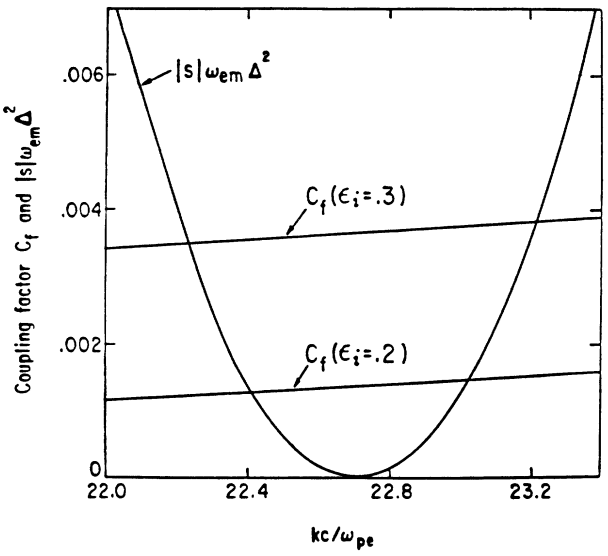


FIG. 3. Coupling factor $C_f$ (straight lines) and $|S|\omega_{em}\Delta^2$ (parabolic curve, $\delta=\Delta/2$ is mismatch) vs wave number for the cases of $\gamma_0=3$, $\theta=45°$, $k_u c/\omega_{pe}=1.6$, and $\epsilon_i=0.2$ and 0.3, respectively.

$$\gamma_{ph}=\left[1-\frac{v_{ph}^2}{c^2}\right]^{-1/2} , \tag{63}$$

$$v_{ph}=v_0-\frac{|S|}{k_p} , \tag{64}$$

where $v_{ph}$ is the phase velocity of the slow electrostatic beam mode. The efficiency for a cold beam may be estimated to be

$$\eta=\frac{\gamma_0-\gamma_{ph}}{\gamma_0-1} . \tag{65}$$

For $\gamma_0 \gg 1$, the efficiency is

$$\eta \sim \gamma_0^2\frac{|S|}{k_p c} \sim \frac{\omega_{pe}}{2\gamma_0^{3/2}k_u c} . \tag{66}$$

The efficiency of the Raman regime is insensitive to the undulator velocity and is inversely proportional to $\gamma_0^{3/2}$.

## IV. HIGH-GAIN COHERENT COMPTON REGIME OF THE ION-RIPPLE LASER

The difference between the high-gain coherent Compton regime and the high-gain Raman regime is due to the importance of space-charge effects. Quantitatively speaking, it is determined by the relation of the mismatch factor and the space-charge term. As the mismatch factor $\omega-\omega_{es}$ (including the space-charge term) is smaller than the space-charge term $\omega/\gamma_0^{3/2}$, the scaling law of the Raman regime is applicable. In other word, the coherent Compton regime is realized if the mismatch factor $\omega-k_p v_0$ is much greater than the space-charge term.

In the coherent Compton regime, the slow and fast electrostatic beam modes both are involved in the instability; they are strongly coupled and grow together. Therefore, as

$$|\omega-k_p v_0| \gg |S| , \tag{67}$$

we must now keep a third-order approximation to the dispersion relation, Eq. (44),

$$(\omega-\omega_{em})(\omega-k_p v_0)^2=\frac{C_f}{2\omega_{em}} . \tag{68}$$

The radiation frequency is approximately determined by the intersection of the electromagnetic wave and the mean frequency of the beam modes. Since we are interested in an energetic electron beams, $\gamma_0 \gg 1$, the radiant frequency is $\omega \sim 2\gamma_0^2 k_{ir} c\cos\theta$. We let

$$\omega-\omega_{em}=\delta-\Delta , \tag{69}$$

$$\delta=\omega-k_p v_0 , \tag{70}$$

$$\Delta=\omega_{em}-k_p v_0 , \tag{71}$$

then, the dispersion relation (high-gain coherent Compton regime) can be written as

$$\delta^3-\Delta\delta^2=C_{fc} , \tag{72}$$

$$C_{fc}=\frac{C_f}{2\omega_{\rm em}} . \tag{73}$$

If

$$\frac{4\Delta^3}{27C_{fc}}>-1 , \tag{74}$$

Eq. (72) has a pair of complex-conjugate roots and one real root. They are

$$\delta_1=(S_1+S_2)+\frac{\Delta}{3} , \tag{75}$$

$$\delta_2=-\tfrac{1}{2}(S_1+S_2)+\frac{\Delta}{3}+i\frac{\sqrt{3}}{2}(S_1-S_2) , \tag{76}$$

$$\delta_2=-\tfrac{1}{2}(S_1+S_2)+\frac{\Delta}{3}-i\frac{\sqrt{3}}{2}(S_1-S_2) , \tag{77}$$

where

$$S_1=\left[\frac{C_{fc}}{2}\right]^{1/2}[1+\zeta+(1+2\zeta)^{1/2}]^{1/3} , \tag{78}$$

$$S_2=\left[\frac{C_{fc}}{2}\right]^{1/3}[1+\zeta-(1+2\zeta)^{1/2}]^{1/3} , \tag{79}$$

$$\zeta=\frac{2\Delta^3}{27C_{fc}} . \tag{80}$$

The unstable spectrum can be divided into three parameter regimes. For $\Delta^3<-27C_{fc}/4$, there are three stable roots. As $\Delta$ is increasing [for $\Delta>-(27C_{fc}/4)^{1/3}$], the growth rate rapidly increase and peaks at $\Delta=0$. Then, the growth rate slowly decreases with increasing $\Delta$. We are interested in the maximum growth rate, that is, $\omega_{\rm em}-k_p v_0=0$. At this point, the electromagnetic wave and the beam modes are strongly coupled. However, the real part of the mismatch factor $\delta$ is not equal to zero. The imaginary part of the radiation frequency and a small deviation of its real part are provided by the coupling factor. The small deviation of the radiation frequency gives a difference between the beam velocity and the phase velocity of the electrostatic potential; that is, it determines the efficiency. At the maximum growth rate, the radiation frequency is

$$\omega-k_p v_0=-\tfrac{1}{2}C_{fc}^{1/3}+i\frac{\sqrt{3}}{2}C_{fc}^{1/3} , \tag{81}$$

where

$$C_{fc}^{1/3}=\left[\frac{\beta_u^2\omega_{pe}^2 k_u c}{4\gamma_0}\right]^{1/3} . \tag{82}$$

Then, we can rewrite condition (67) to be

$$\left[\frac{\beta_u^2\omega_{pe}^2 k_u c}{4\gamma_0}\right]^{1/2}\gg\frac{\omega_{pe}}{\gamma_0^{3/2}} \tag{83}$$

or

$$\beta_u\gg\left[\frac{\omega_{pe}}{k_u c}\frac{4}{\gamma_0^{7/2}}\right]^{1/2} . \tag{84}$$

If this condition is satisfied, the scaling law of the high-gain coherent Compton regime is applicable and its maximum growth rate is

$$\frac{\omega_{i,\max}}{k_u c}=\frac{\sqrt{3}}{2}\left[\frac{\beta_u^2}{4}\frac{\omega_{pe}^2}{\gamma_0 k_u^2 c^2}\right]^{1/3} . \tag{85}$$

For a monoenergetic electron beam, the efficiency of the high-gain coherent Compton regime can be estimated from electron trapping in the electrostatic potential of the beam modes. From Eq. (81), we know the phase velocity of the beam mode for the maximum growth rate mode is

$$v_{\rm ph}=v_0-\frac{C_{fc}^{1/3}}{k_p} , \tag{86}$$

where the amplitude of the mismatch factor is used. If $C_{fc}^{1/3}/k_u c\gg 1$, using Eq. (65), the efficiency is

$$\eta\simeq\frac{1}{2}\left[\frac{\beta_u^2}{4}\frac{\omega_{pe}^2}{\gamma_0 k_u^2 c^2}\right]^{1/3} . \tag{87}$$

We know that $\omega_{i,\max}/k_u c=\sqrt{3}\eta$ by comparing the efficiency and the maximum growth rate; that is, both these quantities have same parameter dependence. One of the parameters, $\beta_u$, needs further discussions since it depends on different plasma density, energy, and undulator length; the scaling law is thus more complicated than it might seem.

### A. Short-undulator-wavelength domain of high-gain coherent Compton regime

The maximum growth rate and the efficiency given in Eqs. (85) and (87), respectively, depend on the transverse, undulator velocity. As shown in Eq. (48), the transverse undulator velocity also depends on the plasma (and beam) density. For the equilibrium state, the transverse ion-ripple force produces undulations in the beam electron's trajectories. This oscillating motion produces a transverse current $j_x$. This current produces a transverse magnetic field $B_{y0}$ through Ampere's law. This transverse magnetic field crossed with the beam electrons' $z$ velocity produce an undulating force in the transverse, $\hat{\mathbf{x}}$, direction. The force modifies the transverse motion via the equations of motion; it must be computed self consistently with $B$. Thus the ion-ripple force, which must be used in the numerator of Eq. (48), depends on the plasma density. The first term in the denominator arises from the equilibrium undulator force which depends on the beam density; the second term is from the inertial force of the beam electrons. Since the scaling of the oscillation velocity is different for different $k_u,\omega_{pe}$, or $\gamma_0$, we separate them into two domains according the relative importance of the equilibrium undulator force and inertial force of beam electrons.

The short-undulator-wavelength domain is defined as

$$k_u c\gg\frac{\omega_{pe}}{\gamma_0} . \tag{88}$$

The inertial force of the beam electrons is dominant over the ponderomotive force in this domain. This gives the undulation velocity to be

$$\beta_u \sim \frac{\omega_{pe}^2}{\gamma_0 k_u^2 c^2}\epsilon_i \sin\theta \ . \tag{89}$$

The condition, Eq. (67), for the high-gain coherent Compton regime to be applicable becomes

$$\frac{\omega_{pe}}{\gamma_0^{1/2} k_u c}\gamma_0 \left[\frac{\epsilon_i \sin\theta}{2}\right]^{2/3} \gg 1 \ . \tag{90}$$

From this inequality, we note that increasing plasma (and beam) density moves one into the coherent Compton regime, not into the Raman regime. The reason for this is that the undulator velocity (which also depends on the plasma density) becomes larger. This is in contrast to the situation for free-electron lasers.

Once this condition is satisfied, the maximum growth rate is

$$\frac{\omega_{i,\max}}{k_u c} \simeq \frac{\sqrt{3}}{2}\left[\frac{\epsilon_i \sin\theta}{2}\right]^{2/3} \frac{\omega_{pe}^2}{\gamma_0 k_u^2 c^2} \ , \tag{91}$$

and the efficiency is

$$\eta \simeq \frac{1}{2}\left[\frac{\epsilon_i \sin\theta}{2}\right]^{2/3} \frac{\omega_{pe}^2}{\gamma_0 k_u^2 c^2} \ . \tag{92}$$

### B. Long-undulator-wavelength domain of the high-gain coherent Compton regime

When the equilibrium ponderomotive force is comparable to the inertial force of the beam electrons, then we are in the long-undulator-wavelength domain

$$\frac{\omega_{pe}}{\gamma_0^{1/2}} \sim k_{ir} c \cos\theta \gg \frac{\omega_{pe}}{\gamma_0^{3/2}} \ ; \tag{93}$$

the transverse undulator velocity, Eq. (48), becomes

$$\beta_u = \frac{1}{1+\kappa^2}\epsilon_i \sin\theta \ , \tag{94}$$

$$\kappa = \frac{k_u c}{\omega_{pe}/\gamma_0^{1/2}} \ , \tag{95}$$

where $1 \sim \kappa \gg 1/\gamma_0$. The transverse undulator motion is insensitive to the beam energy and its spread. Longer-undulator-wavelengths give stronger undulation velocities. But, the beam radius is required to be larger than the wavelength to satisfy the one-dimensionality assumption. The condition (67) for the coherent Compton regime becomes

$$\frac{\kappa}{1+\kappa^2}\frac{\gamma_0^3}{4} \gg 1 \ . \tag{96}$$

This condition is easily satisfied for a high-energy beam. The radiation frequency is $\omega \sim 2\gamma_0^2 k_{ir} c \cos\theta \sim 2\gamma_0^{3/2}\omega_{pe}$. This scaling is something of a disadvantage to compare with the short-undulator-wavelength domain for using a same electron beam. But, it may be still better than for free-electron lasers (FEL's) since the undulator wavelength may be shorter than that for FEL's. The maximum growth rate and the efficiency are

$$\frac{\omega_{i,\max}}{k_u c} \simeq \frac{\sqrt{3}}{2}\left[\frac{\epsilon_i \sin\theta}{2}\right]^{2/3}\left[\frac{1}{\kappa+\kappa^3}\right]^{2/3} , \tag{97}$$

$$\eta \simeq \frac{1}{2}\left[\frac{\epsilon_i \sin\theta}{2}\right]^{2/3}\left[\frac{1}{\kappa+\kappa^3}\right]^{2/3} . \tag{98}$$

The maximum growth rate and efficiency are much greater than that of the short-undulator-wavelength domain.

We note that there are some problems which need to be considered in the long-undulator-wavelength domain. Since the undulator frequency of the ion-ripple laser is comparable to that of the ion-channel laser (ICL), ion focusing effects may play an important role and need to be studied. However, the results may be better since the ion focusing force may provide beam guiding for the ion-ripple laser, just as an axial magnetic field does for a free-electron laser.

## V. RESULTS OF ELECTROMAGNETIC PARTICLE SIMULATION

We checked the validity of the ion-ripple laser theory using the multidimensional (one dimension in space, three dimensions in momenta and fields) periodic electromagnetic particle-in-cell simulation code [10]. The simulation began in the equilibrium state, given by Eqs. (19)–(25), plus a small amount of random thermal velocity.

The simulation's numerical parameters were as following: the grid size $\Delta x$ is set to 1, the periodic system length is 1024 grids, the time is normalized to $\omega_{pe}^{-1}$, the speed of light is equal to 26, the particle size $a=0.6$, the number of electrons is 10 240, the ions are a motionless background with a given ripple, and the thermal momentum spread is 0.6.

Figure 4 shows the growth rate of em waves vs $k$ for the cases of $\gamma=3$, $k_u c=1.6\omega_{pe}$, $\theta=45°$, and $\epsilon_i=0.3$ and 0.2, respectively. The simulations agree well with the theoretical predictions and verify that increasing the fractional ripple of the ion density (i.e., increasing the coupling factor) makes the growth rate larger and the unstable bandwidth broader as discussed and shown in Fig. 3. The electromagnetic and electrostatic waves' power spectra for the case $\epsilon_i=0.3$ is shown in Fig. 5; at $\omega_{pe}t=500$ both waves have already grown to significant amplitudes. Momentum conservation $k_p=k+k_u$ is satisfied and we also observe that $\omega_{\rm em} \sim \omega_{\rm es}$ (not shown). These results agree with the theory of backward Raman scattering.

The efficiency is defined by the percentage of the initial beam energy converted to the electromagnetic wave energy. The time evolution of the radiation wave energy for the case of $\gamma_0=3$, $\theta=45°$, $k_u c/\omega_{pe}=1.6$, and $\epsilon_i=0.3$ (Fig. 6) gives an efficiency of $\eta \sim 7\%$, while the theoretical estimate gives $\eta \sim 9\%$. An absolute instability of the forward-scattering mode is observed and is believed to be

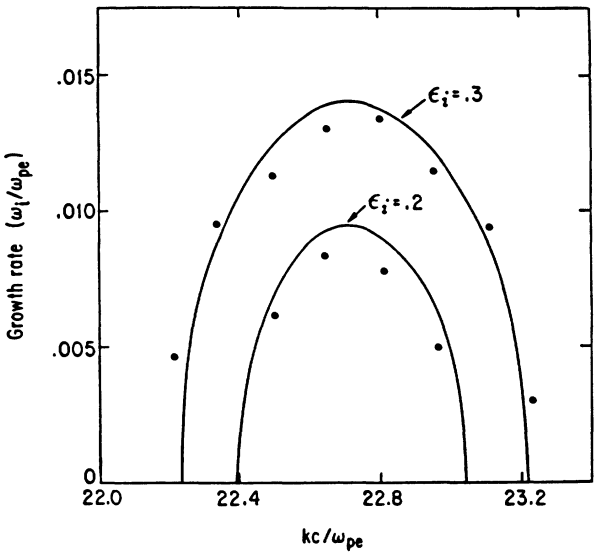


FIG. 4. Growth rate from theory (solid lines) and simulation (discrete points) vs wave number for the cases of $\gamma_0=3$, $\theta=45°$, $k_u c/\omega_{pe}=1.6$, and $\epsilon_i=0.2$ and 0.3, respectively.

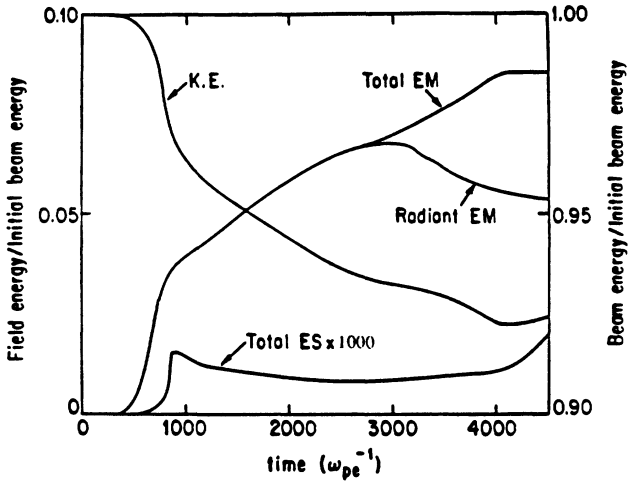


FIG. 6. Time evolution of beam kinetic, total electrostatic, total electromagnetic, and radiant electromagnetic wave energies for the case of $\gamma_0=3$, $\theta=45°$, $k_u c/\omega_{pe}=1.6$, and $\epsilon_i=0.3$. The electrostatic energy is multiplied by a factor of 1000.

responsible for this reduction. The instability of the forward-scattered mode can be decreased by increasing the effective wave number of the ion ripple and/or the beam energy [20,21]. The simulation showed an interesting phenomena, at $t\sim1000$, the wave growth driven by the Raman scattering seems to have reached a peak, the wave begins to grow linearly instead of exponentially. We note that, at that moment, the electron beam has acquired substantial thermal spread; at this time the system should be in the incoherent Compton scattering (negative Landau damping) regime. We also observe that lower wave number em modes grow at later times for this case; this may be due to the beam slowing and/or parasitic parametric instability [22]. This is shown in Fig. 7.

The efficiencies and maximum growth rates of different $k_u c$ are given in Fig. 8 for the case of $\gamma=3$, $\epsilon_i=0.3$, and $\theta=45°$. As the undulator wave number increases, both the efficiency and maximum growth rate decrease. The results of the simulations agree well with theory. Note that the efficiency decreases slower than the growth rate. Figure 9 shows the dependence of efficiency and maximum growth rate on beam energy for the case of $k_u c=1.6$, $\epsilon_i=0.3$, and $\theta=45°$. Both the efficiency and maximum growth rate decrease with increasing the beam energy. The theoretical and simulation results agree well. The theory shows that the decline of efficiency is faster than that of the maximum growth rate.

The effects of beam energy spread on the maximum growth rate and efficiency were also studied. In the simulation, we assign every electron the same beam drift energy. Then, a thermal momentum spread is randomly given to electron. Thus the momentum spread also causes an energy spread; that is, $\Delta P_z/P_{z0}=(\Delta\gamma/\gamma)(1+1/\gamma^2)$.

Figures 10 and 11 show the effects of momentum spread on the maximum growth rate and the efficiency, respectively, for the case of $\gamma_0=3$, $k_u c/\omega_{pe}=1.6$, $\epsilon_i=0.3$, and $\theta=45°$. Even though both of them decrease with increasing momentum spread, the decrease is slow for a few percent of momentum spread. The fractional

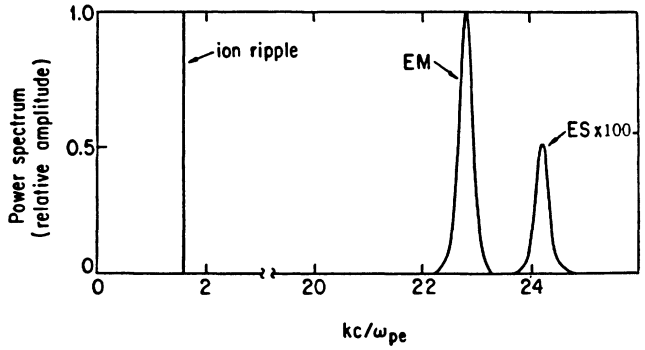


FIG. 5. Unstable electromagnetic (EM) and electrostatic (ES) power spectrum for the case of $\gamma_0=3$, $\theta=45°$, $k_u c/\omega_{pe}=1.6$, and $\epsilon_i=0.3$. The electrostatic amplitude is multiplied by a factor of 100.

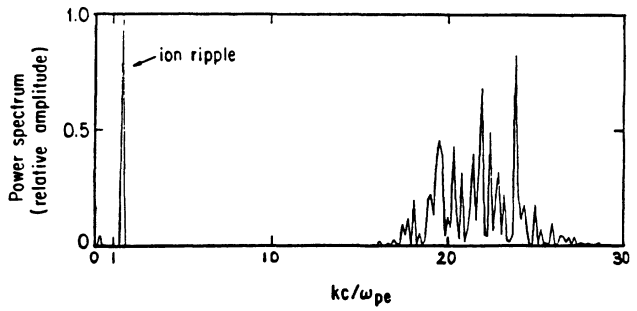


FIG. 7. Unstable electromagnetic waves' power spectrum for the case of $\gamma_0=3$, $\theta=45°$, $k_u c/\omega_{pe}=1.6$, and $\epsilon_i=0.3$. Lower wave-number modes appear in the wave spectrum at later time.

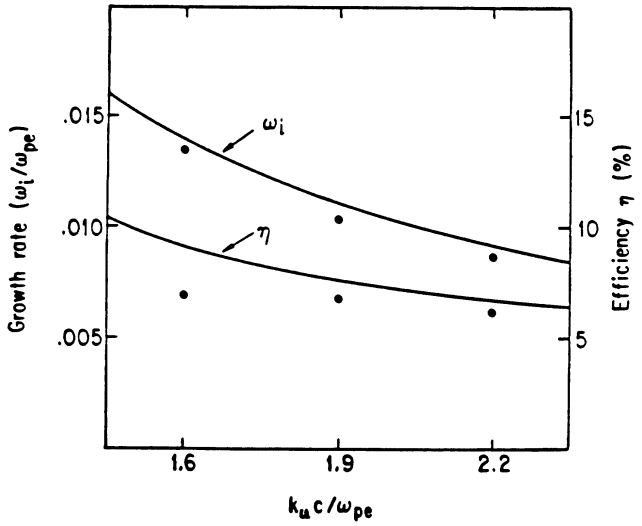


FIG. 8. Maximum growth rate and efficiency from theory (solid lines) and simulation (discrete points) as a function of effective undulator wave number for the case of $\gamma_0=3$, $\theta=45°$, and $\epsilon_i=0.3$.

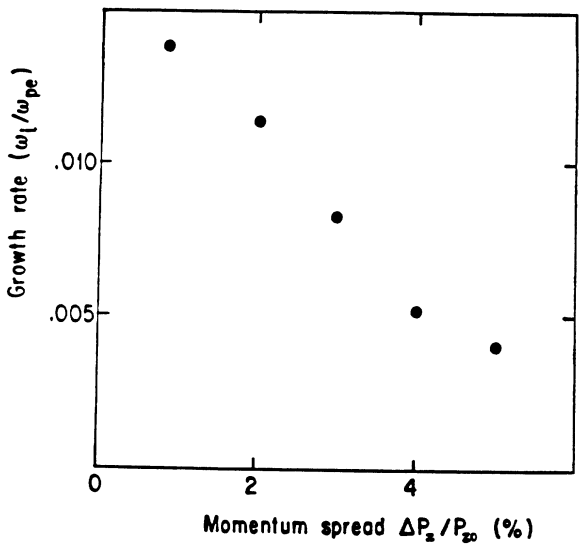


FIG. 10. Maximum growth rate from the simulation as a function of momentum spread $\Delta P_z/P_{z0}$ for the case of $\gamma_0=3$, $k_u c/\omega_{pe}=1.6$, $\theta=45°$, and $\epsilon_i=0.3$.

spread of axial momentum should be smaller than the cold-beam efficiency.

## VI. POSSIBLE APPLICATION OF IRL'S AND COMPARISON WITH FEL'S

Before comparing the ion-ripple laser with FEL's and ICL's and also discussing possible applications of the IRL, we would like to list the condition, for the maximum growth rates, and the efficiencies for three regimes (domains). These are given in Table I for easy comparison. The three regimes are the high-gain Raman regime, the short-undulator-wavelength domain of the high-gain coherent Compton regime, and the long-undulator-wavelength domain of the high-gain coherent Compton regime.

Due to technical limitations of undulator wavelengths (e.g., $\lambda_u \geq 1$ cm) and magnetic-field strength (e.g., $<5\times10^4$ G), conventional FEL requires a very-high-$\gamma$ (e.g., $\sim10^3$) electron beam to produce a short wavelength (e.g., $\lambda\sim500$ Å) and operate there with a low efficiency. This increases many beam requirements: higher energy, higher current, and higher quality as well as the magnet requirements of stronger and more precise magnetic field,

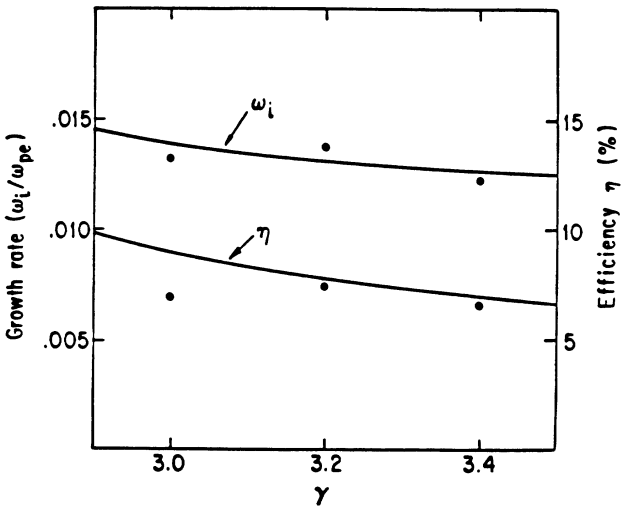


FIG. 9. Maximum growth rate and efficiency from theory (solid lines) and simulation (discrete points) as a function of beam $\gamma_0$ for the case of $k_u c/\omega_{pe}=1.6$, $\theta=45°$, and $\epsilon_i=0.3$.

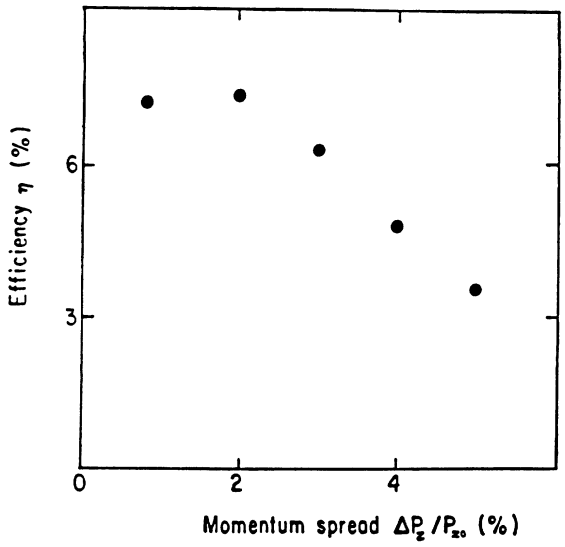


FIG. 11. Efficiency from the simulation as a function of momentum spread $\Delta P_z/P_{z0}$ for the case of $\gamma_0=3$, $k_u c/\omega_{pe}=1.6$, $\theta=45°$, and $\epsilon_i=0.3$.

TABLE I. A list of the validity condition, the maximum growth rate, and the efficiency for high-gain Raman, short-undulator-wavelength coherent Compton, and long-undulator-wavelength coherent Compton regimes.

| | Condition | $\omega_{i,\max}$ | $\eta$ |
|---|---|---|---|
| Raman | $\omega - k_p v_0 \sim \frac{\omega_{pe}}{\gamma_0^{3/2}}$ | $\frac{\omega_{i,\max}}{\omega_{pe}} = \left[\frac{\omega_{pe}}{\sqrt{\gamma_0}k_u c}\right]^{3/2} \frac{\epsilon_i \sin\theta}{2\sqrt{2}}$ | $\frac{\omega_{pe}}{2\gamma_0^{3/2}k_u c}$ |
| Short | $\frac{\omega_{pe}}{\sqrt{\gamma_0}k_u c}\gamma_0 \left[\frac{\epsilon_i \sin\theta}{2}\right]^{2/3} \gg 1$ | $\frac{\omega_{i,\max}}{k_u c} = \frac{\sqrt{3}}{2}\frac{\omega_{pe}^2}{\gamma_0 k_u^2 c^2}\left[\frac{\epsilon_i \sin\theta}{2}\right]^{2/3}$ | $\frac{1}{\sqrt{3}}\frac{\omega_{i,\max}}{k_u c}$ |
| Long | $\frac{\omega_{pe}}{\sqrt{\gamma_0}} \sim k_u c,\ \frac{\kappa}{1+\kappa^2}\frac{\gamma_0^3}{4} \gg 1$ | $\frac{\omega_{i,\max}}{k_u c} = \frac{\sqrt{3}}{2}\left[\frac{1}{\kappa+\kappa^3}\right]^{2/3}\left[\frac{\epsilon_i \sin\theta}{2}\right]^{2/3}$ | $\frac{1}{\sqrt{3}}\frac{\omega_{i,\max}}{k_u c}$ |

very accurate undulator wavelengths and alignment. In addition, the gain and efficiency are small. Neutrons and $\gamma$ rays produced by the energetic beam require elaborate shielding. Although some nonconventional FEL's [23,24] can provide short undulator wavelengths, these have their limitations. ICL's [31,32] can have higher electron oscillation frequencies ($\omega_{pe}/\gamma_0^{1/2}$) and stronger effective fields than conventional FEL's; however, the scaling of the radiation frequency with $\gamma$ (i.e., $\omega \sim 2\gamma_0^{3/2}\omega_{pe}$) is something of a disadvantage.

By employing an IRL, the undulator wave number can be larger (e.g., $k_u c > \omega_{pe} \sim 2.5\times10^{13}$ rad/sec for $n_0 = 1.9\times10^{17}$ cm$^{-3}$) and can easily be adjusted; the ion-ripple field is essentially steady and very high (e.g., $|E_{ir}| \sim 100$ KG for $n_0 = 1.9\times10^{17}$ cm$^{-3}$, $k_{ir}c = 2\omega_{pe}$, and $\epsilon_{ir} = 0.1$). The ion ripple is produced in a neutral plasma, it should be easy to generate and requires little energy; there is no need for an external magnet system. Thus the IRL's using relatively-low-energy beams can provide the same frequencies with higher efficiencies than standard FEL's. Power supplies can be simpler and heavy radiation shield required for very-high-energy beams may be eliminated. Alternatively, an IRL using the same energy beam as an FEL can produce shorter-wavelength coherent radiation.

Beam quality is a major concern for coherent radiation sources, especially at short wavelengths. The ion channel in the ion-ripple laser provides some advantages for the beam emittance requirement. In a FEL, to ensure the maximum geometrical overlap (filling factor) of the radiation field and the electron beam, the emittance of an electron beam is related to the radiation wavelength, that is, $\epsilon = \lambda/\pi$. This is a severe requirement for making an ultraviolet or shorter radiation source. For IRL's, the ion-focusing force can prevent the increase of the electron beam diameter. The radiation can be confined to some degree by dielectric guiding by the plasma since the dielectric constant in the beam is larger than that of the outside plasma due to the relativistic mass increase of its electron. These effects may help with emittance requirements. This whole problem needs much more study. Also, beam emittance gives an effective beam energy spread. The relation is

$$\frac{\Delta\gamma_z}{\gamma_0} \simeq \frac{1}{2}\left[\frac{\epsilon_n}{a}\right]^2, \tag{99}$$

where $\epsilon_n = \beta_0\gamma_0\epsilon$ is the normalized beam emittance, and $a$ is the radial size of the beam.

In addition to the beam emittance, another important aspect is the axial velocity spread (and/or the axial beam energy spread). We can define the scaled velocity spread as

$$V_s = \frac{v_s'}{|v_{ph}'|}, \tag{100}$$

where $v_s'$ is the velocity spread, $v_{ph}'$ is the phase velocity of electrostatic wave, and the superscript denotes the quantities in the beam frame. When $V_s$ approaches 1, the velocity spread approaches the phase velocity of the es mode (or ponderomotive force wave) in the beam frame and, thus, the cold-beam limit breaks down and we must use a warm-beam (kinetic) approximation [9]. Lorentz

TABLE II. Numerical examples of ion-ripple laser scalings in the high-gain Raman regime. The angle between beam and ion ripple is 45° and $k_u c \sim 2\omega_{pe}$.

| | Microwave | Infrared | Ultraviolet | X ray |
|---|---|---|---|---|
| $E$ (MeV) | 1 | 5 | 30 | $2\times10^2$ |
| $\Delta E$ (keV) | $<50$ | $<34$ | $<16$ | $<26$ |
| $I$ (kA) | 1 | 1 | 1 | 4 |
| $n_b$ (cm$^{-3}$) | $8.6\times10^9$ | $4.7\times10^{13}$ | $4.4\times10^{14}$ | $4.0\times10^{15}$ |
| $\lambda_{ir}$ (cm) | 13 | 0.17 | 0.05 | 0.019 |
| $\omega_{i,\max}/\omega_{pe}$ | $4.2\times10^{-3}$ | $1.5\times10^{-3}$ | $4.1\times10^{-4}$ | $1\times10^{-4}$ |
| $\eta$ | $5\times10^{-2}$ | $6.9\times10^{-3}$ | $5.4\times10^{-4}$ | $3.3\times10^{-5}$ |
| $\lambda$ (Å) | $1\times10^8$ | $1\times10^5$ | $1\times10^3$ | 9 |
| $P$ (MW) | 50 | 34 | 16 | 26 |

TABLE III. Numerical examples of ion-ripple laser scalings in the high-gain coherent Compton regime. The angle between beam and ion ripple is 45°.

| | Infrared | Ultraviolet | X ray |
|---|---|---|---|
| $E$ (MeV) | 5 | 30 | $2\times10^{2}$ |
| $\Delta E$ (keV) | $<170$ | $<110$ | $<220$ |
| $I$ (kA) | 1 | 1 | 4 |
| $n_b$ (cm$^{-3}$) | $4.7\times10^{13}$ | $4.4\times10^{14}$ | $4.0\times10^{15}$ |
| $\lambda_{ir}$ (cm) | 1.1 | 0.2 | 0.053 |
| $k_u c/\omega_{pe}$ | 0.3 | 0.5 | 0.7 |
| $\omega_{i,\max}/k_u c$ | $5.9\times10^{-2}$ | $6.1\times10^{-3}$ | $4.8\times10^{-4}$ |
| $\eta$ | $3.4\times10^{-2}$ | $3.6\times10^{-3}$ | $2.8\times10^{-4}$ |
| $\lambda$ (Å) | $6.5\times10^{5}$ | $4.0\times10^{3}$ | 24 |
| $P$ (MW) | 170 | 108 | 224 |

transformation gives the relation of the quantities in the beam frame and laboratory frame as $v_s'=\gamma^2 v_s$ and $v_{\rm ph}'=\gamma^2(v_{\rm ph}-v_0)$. In the laboratory frame,

$$V_s=\frac{v_s}{v_{z0}-v_{\rm ph}} . \tag{101}$$

For $\gamma_s \gg 1$, the scaled velocity spread can also be expressed, in terms of the cold-beam efficiency, as

$$V_s \sim \frac{\gamma_z v_s}{\eta c} \sim \frac{\Delta\gamma}{\gamma\eta} . \tag{102}$$

The fractional spread of axial beam energy is required to be small compared to the efficiency. The efficiency in the coherent Compton regime is proportional to the undulation velocity. In the IRL's, the driving force is stronger and, thus, provides a larger oscillation velocity than in a FEL for the same undulator wavelength. Thus IRL's have higher efficiency and hence allow a larger energy spread. Also, IRL's require lower beam energy than FEL's for the same wavelength radiation. The efficiency for both the coherent Compton and the Raman regime is inversely proportional to $\gamma$ such that a lower beam energy means a larger beam energy spread is allowed.

Table II gives numerical exmaples for the ion-ripple laser scaling from the scaling laws for backward Raman scattering in four frequency regimes for an electron beam whose parameters are accessible with current technology, $\theta=45°$, $\epsilon_i \sim 0.1$, and $k_u c \sim 2\omega_{pe}$. $E$ is the beam energy, $\Delta E$ is the energy spread, $I$ is the beam current, the beam density $n_b$ is assumed to be the same as the plasma (ion) density, $\lambda_{ir}$ is the ripple length, $\lambda$ is the radiation wavelength, and $P$ is the peak output power. The peak power of the radiation is estimated from the Raman scattering scaling law (see Sec. III).

We also give numerical examples from the scaling law for the high-gain coherent Compton scattering regime for the ion-ripple laser for three frqeuency ranges; these are shown in Table III. The electron beam parameters are the same as those used above. The fractional ripple in the ion density and the angle between the electron beam and the ion ripple remain the same. We changed the wavelength of the ion ripple to satisfy the condition for the high-gain coherent Compton regime. The IRL's numerical examples of both coherent Compton and Raman regimes show that high-power, high-efficiency, and short-wavelength lasers may be achieved with relative low energy and quality beams. For instance, to have uv lasing in the coherent Compton regime, the axial beam energy spread is required to be smaller than 0.36%; that is, for a beam $\gamma=60$, the energy spread is required to be smaller than 110 keV. If the beam employed for the uv lasing in Tables II and III has a normalized emittance $\epsilon_n=3\times10^{-4}\pi$ cm rad, the axial energy spread caused by the emittance is about 9 keV (or $\Delta\gamma_z/\gamma_0\sim3.1\times10^{-4}$); it is smaller than that required for the application in both the Raman and the coherent Compton regimes. For the x-ray case in the coherent Compton regime, the beam normalized emittance is required to be smaller than $2\times10^{-4}\pi$ cm rad.

## VII. SUMMARY AND DISCUSSION

We have studied a laser concept which should be capable of producing radiation in the microwave region, in the optical region, or even in the x-ray region by properly choosing parameters. The laser uses a plasma ion ripple for the undulator; the electron beam propagates at an angle to the $k$ vector of the ion ripple. We call this the ion-ripple laser. We believe that the IRL can provide a simple system with high-frequency output, high-efficiency, and output power at relatively modest energies and beam quality; in many situations it may be superior to FELs. Analytic theory and an electromagnetic particle-in-cell simulation code were used to verify the concept and to study the mechanisms of nonlinear saturation, efficiency limits and the effects of momentum spread.

The dispersion relation was derived from fluid theory; the analysis involves radiation and beam mode coupling by the ion ripple; growth rates for unstable modes are obtained. When the slow- and fast-beam space-charge mode can be decoupled, a quadratic equation is obtained and solved to obtain the growth rate and bandwidth for so called "backward Raman scattering." In this case the fast mode is stable. The efficiency is estimated from beam electron trapping in the electrostatic or ponderomotive

potential wells. As the beam energy increases, the number of ion ripples required for the saturation is lower. A multidimensional electromagnetic relativistic particle-in-cell simulation model has been developed to study this problem. The growth rate, frequency bandwidth, nonlinear saturation, and efficiency are found; they agree well with our theoretical predictions. The effect of momentum (energy) spread parallel to the beams direction of propagation was studied.

When space-charge effects are not important, the slow and fast modes both play a role. The coupling of these two modes and the electromagnetic mode gives a cubic equation for high-gain backward coherent Compton scattering. For long-undulator wavelengths, the equilibrium oscillations of the beam electrons produce currents and magnetic fields which modify the undulator force; this occurs only when the beam radius is large compared to the ripple wavelength. The conditions required for the high-gain coherent Compton regime to be valid are given. As the plasma (and beam) density becomes large, it becomes more likely to operate in the high-gain coherent Compton regime than in the Raman regime. This is because the pump field is stronger. The high-gain condition for the long-undulator-wavelength domain is easily satisfied, but the scaling of radiation frequency with energy is less favored. The maximum growth rate ($\omega_{i,\max}/k_u c$) and the efficiency have the same parameter scaling. Since the high-gain coherent Compton regime usually requires a high-beam $\gamma$, new particle simulation codes, such as a moving frame code, need to be developed to fully investigate it.

The electron beam produces an ion channel, whose focusing force can guide the beam. The channel has a higher dielectric constant than the surrounding plasma (because of the relativistic mass increase) and this can act as a waveguide for the radiation generated. To study this effect will require a two-dimensional in space and three-dimensional in momenta and fields electromagnetic code.

Since ion ripples can be created with very short wavelengths and the effective undulator field is quite high, we expected the IRL to be a realistic means for generating short-wavelength tunable coherent lasers; it may even prove practical to produce x rays by this means. Furthermore, the channel effect can reduce emittance requirement and the high efficiency can allow larger axial energy spread; that is, the requirements on beam quality may be lower than for FEL's. Proof of principal experiments are called for; these may begin with low-frequency devices.

The scaling law shown in this paper are for a uniform ion ripple and a plane electromagnetic wave. Tapering of the ripple wavelength and the effects of partial dielectric waveguiding may enhance lasing. A shorter wavelength can be achieved by increasing the undulator wave number and/or the beam energy and by adjusting the angle of beam injection.

One problem that may arise is the following. The theory given is derived from a fluid model for the beam electrons. We note that, for a wavelength equal to or shorter than x rays, the electron spacing ($n_b^{-1/3}$) may be larger than the radiation wavelength so the theory may be called into question. However, the linear density of a 1-kA beam is $2.1\times10^{11}$ cm$^{-1}$; that is, there are more than $10^4$ particles per wavelength for $\lambda\sim5$ Å. Thus we expect the collective picture to hold for the essentially plane waves we are trying to generate.

Although the lasing mechanism discussed in this paper is applied to laboratory radiation sources with their very coherent beams and waves, the mechanism may also occur in nature and particularly in some astrophysical radiation sources.

---

*Present address: Institute for Fusion Studies, University of Texas, Austin, TX 78712.

[1] K. R. Chen and J. M. Dawson, Phys. Rev. Lett. **68**, 29 (1992).
[2] A. E. Dangor *et al.*, IEEE Trans. Plasma Sci. **PS-15**, 161 (1987).
[3] See, for example, N. A. Krall and A. W. Trivelpiece, *Principles of Plasma Physics* (McGraw-Hill, New York, 1973), pp. 108 and 109.
[4] J. J. Su, T. Katsouleas, J. M. Dawson, and R. Fedele, Phys. Rev. A **41**, 3321 (1990).
[5] W. E. Martin *et al.*, Phys. Rev. Lett. **54**, 685 (1985), and references therein.
[6] A. T. Lin, P. K. Kaw, and J. M. Dawson, Phys. Rev. A **8**, 2618 (1973).
[7] C. K. Birdsall, Proc. IRE **42**, 1628 (1954).
[8] K. R. Chen, J. M. Dawson, A. T. Lin, and T. Katsouleas, Phys. Fluids B **3**, 1270 (1991).
[9] T. M. O'Neil and J. H. Malmberg, Phys. Fluid **11**, 1754 (1968).
[10] K. R. Chen and J. M. Dawson, J. Comput. Phys. (to be published).
[11] H. Motz and M. Nakamura, Ann. Phys. (Leipzig) **7**, 84 (1959).
[12] R. M. Phillips, IRE Trans. Electron Devices **7**, 231 (1960).
[13] J. M. J. Madey, J. Appl. Phys. **42**, 1906 (1971).
[14] L. R. Elias, W. M. Fairbank, J. M. J. Madey, H. A. Schwettman, and T. I. Smith, Phys. Rev. Lett. **36**, 717 (1976).
[15] D. A. G. Deacon, L. R. Elias, J. M. J. Madey, G. J. Ramian, H. A. Schwettman, and T. I. Smith, Phys. Rev. Lett. **38**, 892 (1977).
[16] W. B. Colson, Phys. Quantum Electron. **5**, 157 (1978).
[17] P. Sprangle, C. M. Tang, and W. Manheimei, Phys. Rev. Lett. **43**, 1932 (1979).
[18] T. Kwan, J. M. Dawson, and A. T. Lin, Phys. Fluids **20**, 581 (1977).
[19] A. T. Lin and J. M. Dawson, Phys. Rev. Lett. **42**, 1670 (1979).
[20] P. C. Liewer, A. T. Lin, J. M. Dawson, and M. Z. Caponi, Phys. Fluids **24**, 1364 (1981).
[21] P. C. Liewer, A. T. Lin, and J. M. Dawson, Phys. Rev. A **23**, 1251 (1981).
[22] A. T. Lin, Phys. Rev. Lett. **46**, 1515 (1981).

[23] L. R. Elias, Phys. Rev. Lett. **42**, 977 (1979).
[24] G. Bekefi, J. S. Wurtele, and I. H. Deutsch, Phys. Rev. A **34**, 1228 (1986).
[25] Y. T. Yan and J. M. Dawson, Phys. Rev. Lett. **57**, 1599 (1986).
[26] J. E. Lasala, D. A. G. Deacon, and J. M. J. Madey, Nucl. Instrum. Methods Phys. Res. A **250**, 262 (1986).
[27] W. B. Colson, SPIE Vol., Free-Electron Lasers **738**, 2 (1987).
[28] J. M. Madey (unpublished).
[29] C. W. Roberson and P. Sprangle, Phys. Fluids B **1**, 1 (1989).
[30] C. J. Mckinstrie and D. F. DuBois, Phys. Fluids **31**, 278 (1988). C. J. McKinstrie, *ibid.* **31**, 1273 (1988).
[31] D. H. Whittum, A. M. Sessler, and J. M. Dawson, Phys. Rev. Lett. **64**, 2511 (1990).
[32] K. R. Chen, T. Katsouleas, and J. M. Dawson, IEEE Trans. Plasma Sci. **18**, 837 (1990).